Elsevier Editorial System(tm) for Journal of Computational and Applied Mathematics
Manuscript Draft

Manuscript Number:

Title: Numerical Simulations of Water-Gas Flow in Heterogeneous Porous Media with Discontinuous Capillary Pressures by the Concept of the Global Pressure

Article Type: Research Paper

Section/Category: 65Mxx

Keywords: Immiscible compressible; two-phase flow; global pressure; heterogeneous porous media; finite volume; nuclear waste.

Corresponding Author: Prof. Brahim Amaziane,

Corresponding Author's Institution:

First Author: Brahim Amaziane

Order of Authors: Brahim Amaziane; Mladen Jurak; Ana Zgaljic-Keko

Numerical Simulations of Water-Gas Flow in Heterogeneous Porous Media with Discontinuous Capillary Pressures by the Concept of the Global Pressure

Brahim Amaziane[1,*], Mladen Jurak[2], Ana Žgaljić Keko[3]

September 26, 2011

[1]Université de Pau, Laboratoire de Mathématiques et de leurs Applications, CNRS-UMR 5142, Av. de l'Université, 64000 Pau, France.
[2]Department of Mathematics, University of Zagreb, Bijenicka 30, 10000 Zagreb, Croatia.
[3]Faculty of Electrical Engineering and Computing, University of Zagreb, Unska 3, 10000 Zagreb, Croatia.

Abstract

We present an approach and numerical results for a new formulation modeling immiscible, compressible two-phase flow in heterogeneous porous media with discontinuous capillary pressures. The main feature of this model is the introduction of a new global pressure and it is fully equivalent to the original equations. The resulting equations are written in a fractional flow formulation and lead to a coupled degenerate system which consists of a nonlinear parabolic (the global pressure) equation and a nonlinear diffusion-convection one (the saturation equation) with nonlinear transmission conditions at the interfaces that separate different media. The resulting system is discretized using a vertex-centred finite volume method combined with pressure and flux interface conditions for the treatment of heterogeneities. An implicit Euler approach is used for time discretization. A Godunov-type method is used to treat the convection terms and the diffusion terms are discretized by piecewise linear conforming finite elements. We present numerical simulations for three one-dimensional benchmark tests to demonstrate the ability of the method to approximate solutions of water-gas equations efficiently and accurately in nuclear underground waste disposal situations.

Keywords: Immiscible compressible, two-phase flow, global pressure, heterogeneous porous media, finite volume, nuclear waste.

* Corresponding author.

1 Introduction

Numerical modeling of multiphase flow in porous media is significant for many petroleum and environmental engineering problems. More recently, modeling multiphase flow received an increasing attention in connection with the disposal of radioactive waste and sequestration of CO_2.

In this paper, we focus our attention on the numerical simulations and modeling of immiscible compressible two-phase flow in porous media with several rock types, in the framework of the geological disposal of radioactive waste. As a matter of fact, one of the solutions envisaged for managing waste produced by nuclear industry is to dispose it in deep geological formations chosen for their ability to prevent and attenuate possible releases of radionuclides in the geosphere. In the frame of designing nuclear waste geological repositories, a problem of possible two-phase flow of water and gas, mainly hydrogen, appears, for more details see for instance [30].

The usual set of equations describing this type of flow is given by the mass balance law and Darcy-Muscat's law for each phase, which leads to a system of strongly coupled nonlinear partial differential equations. In such systems there are several choices of primary variables. In this work we will use the fractional flow formulation which employs the global pressure and the water saturation as main unknowns. The global pressure has been used in a wide range of numerical simulations, especially in hydrology and petroleum reservoir engineering, see for instance [11, 14] and the references therein.

In the case of immiscible compressible two-phase flow, the concept of the global pressure has not been applied until recently. An exception is its application in certain approximative models, see [11] and the references therein. Since comparisons with other formulations [14] have shown the computational effectiveness of the global pressure, it is worthwhile to investigate its effectiveness in the compressible flow case. Recently, a fully equivalent global pressure formulation to the original equations for water-gas flow was derived in [3] and for the two compressible fluids case, it was developed in [4]. In [5], it was shown that this global pressure formulation is more suitable for the mathematical analysis of two-phase immiscible compressible flow through heterogeneous porous media and, under some realistic assumptions on the data, an existence result was obtained. Let us also mention that for the three-phase compressible flows case, a global pressure formulation fully equivalent to the original equations was derived in [12], and afterwards considered in [15].

In the subsurface, these processes are complicated by the effects of heterogeneity on the flow and transport. Simulation models, if they are intended to provide realistic predictions, must accurately account on these effects. Here, we will assume that the porous medium is composed of multiple rock types, i.e. porosity, absolute permeability, relative permeabilities and capillary pressure curves being different in each type of porous media. Such heterogeneous porous media lead to a possibly discontinuous solution at medium interfaces, which is a consequence of the transmission conditions at the interfaces. This should be taken into account in the discretization. In [16], by analyzing a one dimensional incompressible flow without gravity, an interface condition for the wetting phase saturation

is derived, which is called the extended capillary pressure condition. If the phase is mobile across the interface, the corresponding pressure is continuous. This was discussed for the incompressible case for a phase formulation in [28] together with theoretical and numerical analysis of the derived problem. In the incompressible case, an interface condition for the global pressure was discussed in [7].

The numerical modeling and analysis of two-phase flow in porous media has been a problem of interest for many years and many methods have been developed. There is an extensive literature on this subject. We will not attempt a literature review here, but merely mention a few references. We refer to the books [11, 14, 21] and the references therein. Several authors have examined numerical simulations of immiscible incompressible (see for instance [21, 7, 8, 1, 18]) and also compressible two-phase flows [2, 13]. In the area of multicomponent models numerical simulations were presented in [6, 9].

Finite volume methods which employ also interface conditions, were studied in the incompressible case by many authors, see for instance [22, 7, 31, 29, 24, 18, 10].

A discontinuous Galerkin method including interface conditions, was considered in the incompressible case in heterogeneous porous media by [19]. Mixed finite element methods combined with the discontinuous Galerkin methods in heterogeneous porous media were studied in the incompressible case by [23, 27].

In the incompressible case, numerical codes applied to two-phase immiscible flow equations can be verified by semi-analytical solutions which allows to investigate the accuracy of numerical schemes. We refer to [17] for a heterogeneous case with no capillary effects, and to [20] for a heterogeneous case including both capillary and advective effects with a simple discontinuity. For compressible models, there is no analytical solution and a numerical method such as finite volume should be used. Verification of numerical models for immiscible compressible flow in porous media by the means of appropriate benchmark problems is a very important step in developing and using these models. We restrict our attention to water (incompressible) and gas (compressible) such as hydrogen in the context of gas migration through engineered and geological barriers for a deep repository for radioactive waste. Recently, the French research group MOMAS (http://www.gdrmomas.org/) has proposed benchmark tests [26] to improve the simulation of the migration of hydrogen produced by the corrosion of nuclear waste packages in an underground storage.

The model to be presented in this paper is formulated in a fractional flow formulation in terms of the global pressure and the wetting (water) phase saturation. This formulation leads to a coupled system consisting of a nonlinear parabolic equation for the global pressure and a nonlinear degenerate parabolic diffusion-convection equation for the water saturation, subject to appropriate boundary and initial conditions. Our aim is to study a fully implicit finite volume scheme for the 1-D problem where a special discretization at the interfaces is developed and present numerical simulations for three of the MOMAS benchmark tests.

The rest of the paper is organized as follows. In section 2 we give a short description of the mathematical model [4] used in this study. The space discretization is performed using a vertex-centred finite volume method and an implicit Euler approach is used for time discretization, and the nonlinear system is solved by Newton-Krylov's method at each

time step. The scheme is presented in section 3 and different types of boundary conditions are discussed. Furthermore, special attention is given to the treatment of the interface conditions in the case of multiple rock types. To validate the efficiency and the accuracy of the method, three 1-D benchmark tests are investigated in section 4 for water-gas flows in highly heterogeneous porous media. In the first test, a partially saturated domain made of two porous media separated by an interface is considered, and hydrogen is injected at the left part of the domain. The second test addresses the evolution of gas migration through a domain composed of two media. The system stars from a non-equilibrium state under high capillary pressures discontinuity and the right part of the domain is saturated by water. The third test case is chosen to test the ability of the method to approximate solutions in a saturated domain composed of two media with different entry pressure in each medium. Lastly, some concluding remarks are forwarded.

2 Mathematical Formulation

We consider two-phase immiscible compressible flow in a porous medium under isothermal condition. The porous medium is assumed to be incompressible with porosity Φ and absolute permeability $\mathbb{K}$. We consider a system in which each component only appears in one of the phases with no mass transfer between the phases. Differential equations describing immiscible, compressible, two-phase flow in a porous medium are given by the mass balance equation for each phase and the Darcy law which relates the phase pressure gradient and volumetric phase velocity (see, e.g., [11, 14, 21]). Different wetting properties of the two fluid phases are described by macroscopic capillary pressure law in which we distinguish the wetting phase, denoted by the subscript w, and the non-wetting phase, denoted by the subscript g.

We denote by $\rho_\alpha(P_\alpha)$ and $\lambda_\alpha(S_\alpha)$, $\alpha \in \{w, g\}$, mass densities and mobilities of each phase, where P_α and S_α are the α-phase pressure and saturation. Phase saturations satisfy

$$S_w + S_g = 1, \tag{1}$$

and they follow the capillary pressure law

$$P_c(S_w) = P_g - P_w, \tag{2}$$

where $P_c(S_w)$ is the capillary pressure function. The mass balance equations and the Darcy law for each phase $\alpha \in \{w, g\}$ can be written as

$$\Phi \frac{\partial}{\partial t}(\rho_\alpha(P_\alpha)S_\alpha) + \operatorname{div}(\rho_\alpha(P_\alpha)\mathbf{q}_\alpha) = \mathcal{F}_\alpha, \quad \mathbf{q}_\alpha = -\lambda_\alpha(S_\alpha)\mathbb{K}(\nabla P_\alpha - \rho_\alpha(P_\alpha)\mathbf{g}), \tag{3}$$

where $\mathbf{g}$ is the gravitational, downward-pointing, constant vector and $\mathcal{F}_\alpha$ the source term. We assume that the porosity and the permeability depend only on the space variable $\mathbf{x}$.

In the sequel, we will use a global pressure formulation that removes the nonlinear capillary pressure gradient term from the total flux. The two-phase flow equations are

written in a fully equivalent global pressure formulation in [3, 4], where a new variable P called the global pressure is introduced with the aim to partially decouple the two mass conservation equations. Phase pressures can then be expressed as functions of the global pressure and saturation, namely, $P_g = P_g(S_w, P)$ and $P_w = P_w(S_w, P)$, where here and in the following we use the same letter for the function and the variable.

In order to write down the system of equations describing the two-phase flow in primary variables S_w and P we introduce the following coefficients ($\alpha \in \{w, g\}$):

$$\rho_w(S_w, P) = \rho_w(P_g(S_w, P) - P_c(S_w)), \quad \rho_g(S_w, P) = \rho_g(P_g(S_w, P)), \tag{4}$$

$$\lambda(S_w, P) = \rho_w(S_w, P)\lambda_w(S_w) + \rho_g(S_w, P)\lambda_g(S_w), \tag{5}$$

$$f_w(S_w, P) = \frac{\rho_w(S_w, P)\lambda_w(S_w)}{\lambda(S_w, P)}, \quad f_g(S_w, P) = \frac{\rho_g(S_w, P)\lambda_g(S_w)}{\lambda(S_w, P)}, \tag{6}$$

$$\rho(S_w, P) = \frac{\lambda_w(S_w)\rho_w(P_w, P)^2 + \lambda_g(S_w)\rho_g(S_w, P)^2}{\lambda(S_w, P)}, \tag{7}$$

$$a(S_w, P) = -\frac{\rho_w(S_w, P)\rho_g(S_w, P)\lambda_w(S_w)\lambda_g(S_w)P_c'(S_w)}{\lambda(S_w, P_g)}, \tag{8}$$

$$b_g(S_w, P_g) = (\rho_w(S_w, P) - \rho_g(S_w, P))\frac{\rho_w(S_w, P)\rho_g(S_w, P)\lambda_w(S_w)\lambda_g(S_w)}{\lambda(S_w, P_g)}. \tag{9}$$

Here, as in [4], the function $P_g(S_w, P)$ is taken as a solution of the integral equation

$$P_g(S_w, P) = P + P_c(1) + \int_1^{S_w} f_w(s, P)P_c'(s)\, ds \tag{10}$$

(here $f_w(s, P)$ is a function of $P_g(s, P)$), and additionally we have

$$P_w(S_w, P) = P_g(S_w, P) - P_c(S_w). \tag{11}$$

The function ω is defined by (see [4])

$$\omega(S_w, P) = \frac{\partial P_w(S_w, P)}{\partial P} = \frac{\partial P_g(S_w, P)}{\partial P},$$

and it is given by the following formula:

$$\omega(S_w, P) = \exp\left(\int_{S_w}^1 (\nu_g(s, P) - \nu_w(s, P))\frac{\rho_w(s, P)\rho_g(s, P)\lambda_w(s)\lambda_g(s)P_c'(s)}{(\rho_w(s, P)\lambda_w(s) + \rho_g(s, P)\lambda_g(s))^2}\, ds\right), \tag{12}$$

where $\omega(1, P) = 1$, as a consequence of $P_g(1, P) = P + P_c(1)$ and, where the fluid compressibilities are defined as:

$$\nu_w(S, P) = \frac{\rho_w'(P_g(S, P) - P_c(S))}{\rho_w(P_g(S, P) - P_c(S))}, \quad \nu_g(S, P) = \frac{\rho_g'(P_g(S, P))}{\rho_g(P_g(S, P))}. \tag{13}$$

The differential equations of the two-phase, compressible, immiscible flow (3) can now be written as (cf. [3, 4]):

$$\Phi\frac{\partial}{\partial t}(S_w\rho_w(S_w,P)+\rho_g(S_w,P)(1-S_w)) \tag{14}$$
$$-\operatorname{div}\Big(\lambda(S_w,P)\mathbb{K}(\omega(S_w,P)\nabla P-\rho(S_w,P)\mathbf{g})\Big)=\mathcal{F}_w+\mathcal{F}_g,$$
$$\mathbf{Q}=-\lambda(S_w,P)\mathbb{K}(\omega(S_w,P)\nabla P-\rho(S_w,P)\mathbf{g}), \tag{15}$$
$$\Phi\frac{\partial}{\partial t}(S_w\rho_w(S_w,P))+\operatorname{div}(f_w(S_w,P)\mathbf{Q}+b_g(S_w,P)\mathbb{K}\mathbf{g})=\operatorname{div}(a(S_w,P)\mathbb{K}\nabla S_w)+\mathcal{F}_w. \tag{16}$$

The pressure equation (14) is a nonlinear parabolic equation, and the saturation equation (16) is convection-diffusion one. The main advantage of (14)-(16) over other equivalent formulations obtained by simple manipulations from the original equations is that the coupling between the two PDEs is much less strong. Furthermore, the form of the system is more adapted for the mathematical and numerical analysis.

3 A Finite Volume Scheme

Finite volume methods are a popular tool for solving partial differential equations. The main property of a finite volume method is the local conservation property on discrete control volumes. Those methods are therefore well suited for the discretization of equations that arise from conservation laws.

Discretization of the coupled system (14)-(16) is performed by a vertex-centred finite volume method, see, e.g., [1], with a fully implicit time stepping. The convective terms are approximated with the aid of a Godunov scheme, where as the diffusion terms are discretized by piecewise linear conforming finite elements.

In this section, we present this finite volume scheme for the 1-D problem in a domain made of multiple rock types. The discontinuity of the saturation at the interface separating two media, as a result of the capillary pressure continuity, may arise from the contrast in the capillary pressure functions leading to complications in numerical modeling. Thus, at each time step one has to solve nonlinear transmission conditions at the interfaces. We employ the Newton method to solve the nonlinear system at each time step. The interface conditions are incorporated into the discretization when we compute the Jacobian and residual in the Newton iterations.

In this and the following sections we will omit the subscript w and we will denote the wetting phase saturation by S.

3.1 Basic Notation

The equations (14)-(16) are solved in a finite time interval $J=]0,T[$, and in a finite spatial domain $I=]a,b[$. In order to present the discretization, the following notation is applied, similar to the one presented in [2]:

(N.1) Let $\left\{t^0 < t^1 < \ldots < t^{N_T}\right\}$ be the discretization of the time domain and we denote by $J_k = [t^k, t^{k+1}[$ the k-level time interval. The time step is: $\triangle t^k = t^{k+1} - t^k$, $k = 0, 1, \ldots, N_T - 1$.

(N.2) Let $\{x_0 < x_1 < \ldots < x_{N_x}\}$ be the discretization of the spatial domain where: $E_{i+\frac{1}{2}} := [x_i, x_{i+1}]$, $i = 0, 1, \ldots, N_x - 1$, as shown in Figure 1 and we set $\triangle x_{i+\frac{1}{2}} = |E_{i+\frac{1}{2}}| = x_{i+1} - x_i$, $i = 0, 1, \ldots, N_x - 1$.

(N.3) Control volumes are defined as follows: for each $i = 0, 1, \ldots, N_x - 1$ we denote the center of the element $E_{i+\frac{1}{2}}$ by $x_{i+\frac{1}{2}} := \frac{x_i + x_{i+1}}{2}$, and set $x_{-\frac{1}{2}} = x_0$ and $x_{N_x+\frac{1}{2}} = x_{N_x}$. For $i = 0, \ldots, N_x$, the control volume is defined as $V_i = [x_{i-\frac{1}{2}}, x_{i+\frac{1}{2}}]$. The following notation is used: $h_i = |V_i| = x_{i+\frac{1}{2}} - x_{i-\frac{1}{2}}, \quad i = 0, 1, \ldots, N_x$.

(N.4) The permeability and the porosity are functions of the space and they are assumed to be constant by element: $K_{i+\frac{1}{2}} = K\big|_{E_{i+\frac{1}{2}}}$, $\Phi_{i+\frac{1}{2}} = \Phi\big|_{E_{i+\frac{1}{2}}}$ $i = 0, 1, \ldots, N_x - 1$.

(N.5) The approximations of S and P at the point (x_i, t_k) are denoted by S_i^k and P_i^k.

A special care has to be taken when the spatial mesh is created in the situations with multiple rock types since in each rock type the rock properties differ. Relative permeabilities and capillary pressure functions may be different for each rock type as well.

If the spatial domain in one dimension is divided into N_m parts, and each part of the domain is related to a certain rock type, there are $N_m - 1$ interfaces. Every interface point is set to be an element of the spatial mesh $\{x_0 < x_1 < \ldots < x_{N_x}\}$. The other nodes of the spatial mesh can be chosen arbitrarily. The numerical scheme will be presented for the situation of the two rock types. A higher number of media does not change the way of the treatment of heterogeneity. In two and three-dimensional case the treatment of the heterogeneity is essentially the same, but technically more complicated. In the following, it is assumed that the spatial domain is divided into two parts, one related to the material $m1$ and the other related to the material $m2$, as is presented in Figure 1.

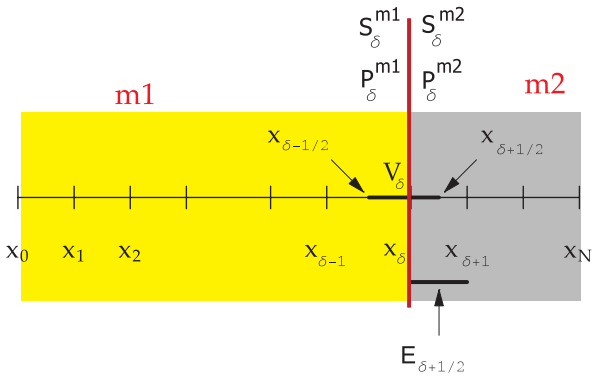

Figure 1: Spatial mesh in one-dimensional case with two rock types.

Let $I = I_{m1} \cup I_{m2}$ and the interface node is set to be $\{x_\delta\} = \overline{I}_{m1} \cap \overline{I}_{m2}$, for an index $\delta \in \{1, 2, \ldots, N_x - 1\}$.

The following functions are introduced:

$M(S,P) := \rho_w(S,P)S + \rho_g(S,P)(1-S)$, $N(S,P) := \rho_w(S,P)S$, $\chi(S,P) := \lambda(S,P)\omega(S,P)$, and the function $\gamma(S,P)$ to satisfy $a(S,P) = \gamma(S,P)P_c'(S)$.

The equations (14)-(16) (with neglected gravity term, for simplicity) rewritten in one-dimensional case, and considering the notation above, are:

$$\Phi \frac{\partial}{\partial t}\left(M(S,P)\right) - \frac{\partial}{\partial x}\left(\chi(S,P)K\frac{\partial P}{\partial x}\right) = \mathcal{F}_w + \mathcal{F}_g, \tag{17}$$

$$Q = -\chi(S,P)K\frac{\partial P}{\partial x}, \tag{18}$$

$$\Phi \frac{\partial}{\partial t}(N(S,P)) + \frac{\partial}{\partial x}\left(f_w(S,P)Q\right) - \frac{\partial}{\partial x}\left(\gamma(S,P)K\frac{\partial P_c(S)}{\partial x}\right) = \mathcal{F}_w. \tag{19}$$

The capillary pressure functions and the relative permeabilities differ on different media. The coefficients of the equations (17)-(19) are calculated from the relative permeabilities and the capillary pressure, therefore, the index m (either $m = m1$ or $m = m2$) will be used to indicate the part of the domain (medium) on which the calculations are done. For every function f depending on the wetting phase saturation and the global pressure we set

$$f(S(x,t),P(x,t)) = \begin{cases} f^{m1}(S(x,t),P(x,t)) & x \in I_{m1} \\ f^{m2}(S(x,t),P(x,t)) & x \in I_{m2} \end{cases}.$$

At the initial time, either the global pressure, the saturation or the phase pressures are given. A set of boundary conditions of diverse types can be given.

Since a porous medium with multiple rock types is considered, the numerical scheme has to employ also the interface conditions for the main unknowns. This is discussed in the following subsection.

3.2 Interface Conditions

In this subsection we will formulate the interface conditions, for the model explained in section 2. Note that we have denoted by S the wetting phase saturation. Let us consider the case when the entry pressure is present in the model so that $P_c^{m1}(1) = P_d^{m1}$ and $P_c^{m2}(1) = P_d^{m2}$. In the situations where $P_d^{m1} \leq P_d^{m2}$, as presented in Figure 2 the interface conditions which connects the limiting saturations on the different materials is given by the extended capillary pressure condition [28]:

$$S^{m2} = \begin{cases} 1 & \text{for } S^{m1} > S^* \\ (P_c^{m2})^{-1}(P_c^{m1}(S^{m1})) & \text{for } S^{m1} \leq S^*, \end{cases} \tag{20}$$

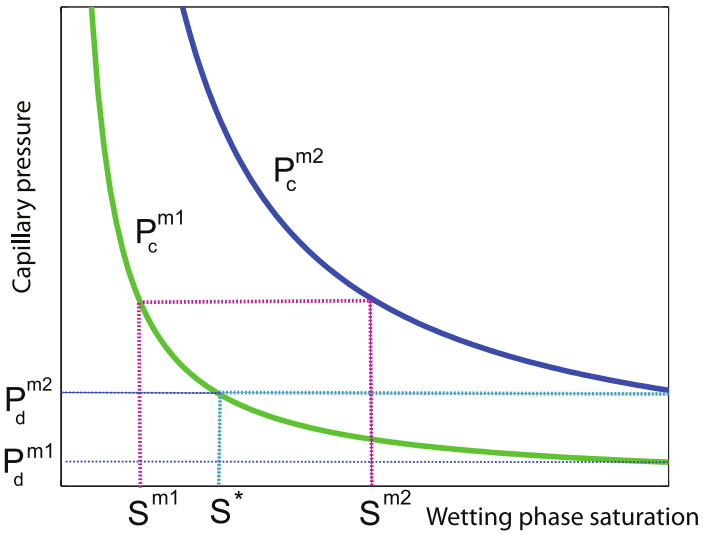

Figure 2: Capillary pressure curves with different entry pressures.

where S^* is a threshold saturation defined by the formula

$$S^* = (P_c^{m1})^{-1}(P_d^{m2}). \tag{21}$$

For the global pressure, the interface condition is derived from the transmission condition for the phase pressures. Similar to [7], where the incompressible case was considered, we have two different cases:

(C.1) $S^{m1} > S^*$, $S^{m2} = 1$; in this situation, the non-wetting pressure is not defined in the domain I_{m2} and P_w is continuous at the interface. Thus, from $P_w^{m2}(1, P) = P$ and from the continuity of the wetting phase pressure we get:

$$P_w^{m1}(S^{m1}, P^{m1}) = P_w^{m2}(1, P^{m2}) = P^{m2}. \tag{22}$$

In this case, the transmission condition between two limiting values of the global pressure is described by the nonlinear equation (22). From given P^{m1} and S^{m1}, the value P^{m2} can be calculated by (22). In reverse, for given P^{m2} and S^{m1} we can compute P^{m1} by solving the nonlinear equation (22), for which the solution is defined since the derivative of the wetting phase pressure over the global pressure is strictly positive.

(C.2) $S^{m1} \leq S^*$, $P_c^{m1}(S^{m1}) = P_c^{m2}(S^{m2})$; here the phase pressures are continuous across the interface, using the continuity of the non-wetting phase pressure, for example, we obtain the following condition for the global pressure:

$$P_g^{m1}(S^{m1}, P^{m1}) = P_g^{m2}(S^{m2}, P^{m2}). \tag{23}$$

In this case, when S^{m1} and S^{m2} are given, we obtain P^{m2} from any given P^{m1} by solving the nonlinear equation (23) whose solution is well defined since the partial derivative of the non-wetting phase pressure over the global pressure is strictly positive. Also, for any given P^{m2} one may calculate P^{m1} from the nonlinear equation (23).

Remark 1. *Note that in the case of the van Genuchten functions the case (C.2) always applies.*

The saturation and the global pressure are generally discontinuous at the interface point. Let us explain the meaning and use of the global unknowns S_δ^k, P_δ^k which we will include in the numerical scheme, as a value of the saturation and the global pressure at the interface node x_δ, at the time level k.

There are several ways of defining these global unknowns. For the saturation the global variable S_δ can be chosen equal to S_δ^{m1} or S_δ^{m2} in advance or as $S_\delta = f(S_\delta^{m1}, S_\delta^{m2})$, where f is strictly increasing function in each variable. Then, in all calculations one can recalculate other limiting value by (20) and perform the calculations with correct limiting value. This also guarantees that during the calculation we actually always work with the correct capillary pressure at the interface node x_δ.

In the simulations where the entry pressure is present (e.g. Brooks and Corey capillary pressure), the choice of the unknown S_δ is more restrictive. If we decide that, during the whole simulation it is equal to the one limiting value, it has to be taken equal to the limiting saturation of the medium which is related to the smaller "entry pressure".

The situation with the global pressure is similar. The choice of P_δ can be done in several ways, and the simplest approach is to choose $P_\delta = P_\delta^{m1}$ or $P_\delta = P_\delta^{m2}$, and then use (22) or (23) depending which of the cases (C.1) or (C.2) applies in order to obtain the other limiting value, depending on which part of the domain the calculation is done.

3.3 Numerical Scheme Presentation

For the presentation of the numerical scheme, we will assume that the value $P_c^{m1}(1) \leq P_c^{m2}(1)$, and for the global unknowns S_δ^k and P_δ^k we will choose the following:

$$S_\delta^k = S_\delta^{m1,k}, \quad P_\delta = P_\delta^{m1,k}.$$

For any function $f(S,P)$ and $j = \pm\frac{1}{2}$, $i = 1, \ldots, N_x - 1$, we define:

$$f_{i+j}^k = f(S_{i+j}^k, P_{i+j}^k),$$

where for $i + j \neq \delta + \frac{1}{2}$, we use the following notation:

$$S_{i+j}^k = \frac{S_i^k + S_{i+2j}^k}{2}, \quad P_{i+j}^k = \frac{P_i^k + P_{i+2j}^k}{2}.$$

If $i + j = \delta + \frac{1}{2}$ we need to use correct limiting values for the saturation and the global pressure. These limiting values are obtained as functions $S_\delta^{m2,k} = S_\delta^{m2,k}(S_\delta^k), P_\delta^{m2,k} =$

$P_\delta^{m2,k}(S_\delta^k, P_\delta^k)$ using the nonlinear transmission conditions explained in the subsection 3.2. So it is set:

$$S_{\delta+\frac{1}{2}}^k = \frac{S_\delta^{m2,k} + S_{\delta+1}^k}{2}, \quad P_{\delta+\frac{1}{2}}^k = \frac{P_\delta^{m2,k} + P_{\delta+1}^k}{2}.$$

At first, the system (17)-(19) is integrated over the set $V_i \times J_k$ to obtain:

$$\sum_{j=\pm\frac{1}{2}} \int_{V_i \cap E_{i+j}} \Phi \left(M^m(S^{k+1}, P^{k+1}) - M^m(S^k, P^k) \right) dx - \int_{J_k} \sum_{j=\pm\frac{1}{2}} (2j) \chi_{i+j}^m K_{i+j} \left(\frac{\partial P}{\partial x} \right)_{i+j} dt$$
$$= h_i \int_{J_k} (\mathcal{F}_{w,i} + \mathcal{F}_{g,i})\, dt$$
$$\sum_{j=\pm\frac{1}{2}} \int_{V_i \cap E_{i+j}} \Phi \left(N^m(S^{k+1}, P^{k+1}) - N^m(S^k, P^k) \right) dx + \int_{J_k} \sum_{j=\pm\frac{1}{2}} (2j) Q_{i+j}^m f_{w,i+j}^{m,up}\, dt$$
$$= \int_{J_k} \sum_{j=\pm\frac{1}{2}} (2j) \gamma_{i+j}^m K_{i+j} \left(\frac{\partial P_c^m(S)}{\partial x} \right)_{i+j} dt$$
$$+ h_i \int_{J_k} \mathcal{F}_{w,i}\, dt,$$

where either $m = m1$ or $m = m2$ depending on which part of the domain the calculation is done. Now for $i + j \neq \delta + \frac{1}{2}$ the following approximations are used:

$$\left(\frac{\partial P}{\partial x} \right)_{i+j} = 2j \frac{P_{i+2j} - P_i}{\Delta x_{i+j}}, \quad \left(\frac{\partial P_c^m(S)}{\partial x} \right)_{i+j} = 2j \frac{P_c^m(S_{i+2j}) - P_c^m(S_i)}{\Delta x_{i+j}}.$$

If $i + j = \delta + \frac{1}{2}$ one sets:

$$\left(\frac{\partial P}{\partial x} \right)_{\delta+\frac{1}{2}} = \frac{P_{\delta+1} - P_\delta^{m2}}{\Delta x_{\delta+\frac{1}{2}}}, \quad \left(\frac{\partial P_c^m(S)}{\partial x} \right)_{\delta+\frac{1}{2}} = \frac{P_c^{m2}(S_{\delta+1}) - P_c^{m2}(S_\delta^{m2})}{\Delta x_{\delta+\frac{1}{2}}}.$$

On the left side of the equations the mass lumping is applied. The following implicit in time scheme is obtained (here we set $\Delta x_{-\frac{1}{2}} = \Delta x_{N_x-\frac{1}{2}} = \Phi_{-\frac{1}{2}} = \Phi_{N_x-\frac{1}{2}} = 0$):

$$\sum_{j=\pm\frac{1}{2}} \Phi_{i+j} \frac{\Delta x_{i+j}}{2} \frac{M_i^{m,k+1} - M_i^{m,k}}{\Delta t^k} = R_{P,i}^{k+1} \tag{24}$$

$$\sum_{j=\pm\frac{1}{2}} \Phi_{i+j} \frac{\Delta x_{i+j}}{2} \frac{N_i^{m,k+1} - N_i^{m,k}}{\Delta t^k} = R_{S,i}^{k+1}, \tag{25}$$

where $m = m1$ or $m = m2$ depending on which part of the domain the calculations are done. The following notation is introduced:

$$T_{i+1/2} := \frac{K_{i+1/2}}{\triangle x_{i+\frac{1}{2}}}, \quad i = 0, 1, 2 \ldots, N_x - 1.$$

For $i = 1, 2, \ldots, N_x - 1$, the right hand side of (24) is

$$R_{P,i}^{k+1} = -\sum_{j=\pm\frac{1}{2}} Q_{i+j}^{m,k+1} + h_i(\mathcal{F}_{g,i}^{k+1} + \mathcal{F}_{w,i}^{k+1}). \tag{26}$$

For $i + j \neq \delta + \frac{1}{2}$, we set

$$Q_{i+j}^{m,k+1} = -\chi_{i+j}^{m,k+1} T_{i+j}(P_{i+2j}^{k+1} - P_i^{k+1}),$$

where either $m = m1$ or $m = m2$, otherwise

$$Q_{\delta+\frac{1}{2}}^{m2,k+1} = -\chi_{\delta+\frac{1}{2}}^{m2,k+1} T_{\delta+\frac{1}{2}}(P_{\delta+1}^{k+1} - P_\delta^{m2,k+1}).$$

For $i = 1, 2, \ldots N_x - 1$

$$R_{S,i}^{k+1} = \sum_{j=\pm\frac{1}{2}} D_{i+j}^{m,k+1} - \sum_{j=\pm\frac{1}{2}} (2j) Q_{i+j}^{m,k+1} f_{w,i+j}^{m,up,k+1} + h_i \mathcal{F}_{w,i}^{k+1}, \tag{27}$$

For $i + j \neq \delta + \frac{1}{2}$, we set

$$D_{i+j}^{m,k+1} = \gamma_{i+j}^{m,k+1} T_{i+j}(P_c^m(S_{i+2j}^{k+1}) - P_c^m(S_i^{k+1})),$$

where either $m = m1$ or $m = m2$, and otherwise we have

$$D_{\delta+\frac{1}{2}}^{m2,k+1} = \gamma_{\delta+\frac{1}{2}}^{m2,k+1} T_{\delta+\frac{1}{2}}(P_c^{m2}(S_{\delta+1}^{k+1}) - P_c^{m2}(S_\delta^{m2,k+1})).$$

For the convective term, the following upwind procedure is applied:

$$f_{w,i+\frac{1}{2}}^{m,up,k+1} = \begin{cases} f_w^m(S_i^{k+1}, P_i^{k+1}) & \text{for } Q_{i+\frac{1}{2}}^{k+1} \geq 0 \\ f_w^m(S_{i+1}^{k+1}, P_{i+1}^{k+1}) & \text{for } Q_{i+\frac{1}{2}}^{k+1} < 0 \end{cases},$$

and note that for $i = \delta$ one has to use the limiting values $P_\delta^{m2,k+1}$ and $S_\delta^{m2,k+1}$ in the above expressions.

The terms $R_{S,0}^{k+1}, R_{p,0}^{k+1}, R_{p,N_x}^{k+1}, R_{S,N_x}^{k+1}$ depend on the imposed boundary conditions.

3.3.1 *Nonlinear Equations*

Notice that by the above discretization procedure a nonlinear system is obtained at each time step which is solved by the Newton method. In order to use this procedure, we need to know how to form a residual and a Jacobian at the previous iteration. While those calculations are done, special attention needs to be paid to the interface node. Considering that all the calculations are performed locally on the element E, it is worthwhile to give some details of the local calculations. A brief explanation is given in the following subsection.

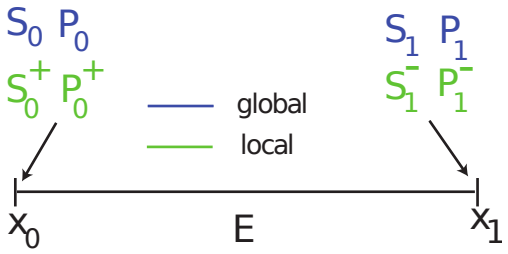

Figure 3: Local and global approximations.

3.4 Local Calculations

All the functions used in the discretization belong to the medium where the current element is positioned. Therefore, the medium index will be omitted in this subsection. Considering that the time index is constant in the scope of this discussion, it is omitted as well. The local calculations are presented for the situation when the phase fluxes are set to be zero at the boundary. For simplicity, in this subsection, it is assumed that $P_d^m = 0,\ m = m1, m2$, and also $\mathcal{F}_w = \mathcal{F}_g = 0$.

Let us denote the local element by $E = [x_0, x_1]$. The values of the global unknowns are set to be P_0, P_1, S_0, S_1. In general we assume that the local values S_0^+, S_1^- depend on the values S_0 and S_1 respectively. Also, we assume, that P_0^+ depends on S_0 and P_0, and that P_1^- depends on P_1 and S_1, see Figure 3.

In the local calculations, the local values $S_0^+, P_0^+, S_1^-, P_1^-$ will be used. As discussed in the previous section, if calculations are performed at the interface node, one needs to know the limit values of the saturation and the global pressure. These are obtained from the global unknown value from the previous iteration. Let us consider the simplest example, if the global unknown for the saturation [resp. the global pressure] at the node x_δ is set to be equal to the left limiting saturation [resp. the global pressure], then it follows:

- $S_1^- = S_1$ is always valid. However, at the point x_0, we set:

$$S_0^+ = \begin{cases} S_0 & \text{if } x_0 \neq x_\delta \\ (P_c^{m2})^{-1}(P_c^{m1}(S_0)) & \text{for } x_0 = x_\delta \end{cases}. \tag{28}$$

- $P_1^- = P_1$ is always valid and at x_0 the calculation has to be performed as follows: assuming S_0^+ is already calculated, we set:

$$P_0^+ = \begin{cases} P_0 & \text{if } x_0 \neq x_\delta \\ \text{solution of } P_g^{m1}(S_0, P_0) = P_g^{m2}(S_0^+, P_0^+) & \text{if } x_0 = x_\delta \end{cases}. \tag{29}$$

For solving this nonlinear equations the Newton method or some other nonlinear solver can be used to obtain the value P_0^+.

The permeability K is constant by element, we set:

$$P_{\frac{1}{2}} = \frac{P_0^+ + P_1^-}{2}, \quad S_{\frac{1}{2}} = \frac{S_0^+ + S_1^-}{2}, \quad dx = x_1 - x_0, \quad T = \frac{K}{dx}.$$

We need to compute the residual local contributions $R_{P,0}, R_{P,1}, R_{S,0}, R_{S,1}$ at the nodes x_0, x_1 at the element E which are added to the global value of the residual. It follows:

$$\begin{aligned} R_{P,0} = &\quad \chi(S_{\frac{1}{2}}, P_{\frac{1}{2}})T(P_1^- - P_0^+) \\ R_{P,1} = &-\chi(S_{\frac{1}{2}}, P_{\frac{1}{2}})T(P_1^- - P_0^+). \end{aligned}$$

For the saturation equation we obtain:

$$\begin{aligned} R_{S,0} &= \gamma(S_{\frac{1}{2}}, P_{\frac{1}{2}})T(P_c(S_1^-) - P_c(S_0^+)) - Q_{\frac{1}{2}} f_w^{up}, \\ R_{S,1} &= -\gamma(S_{\frac{1}{2}}, pP_{\frac{1}{2}})T(P_c(S_1^-) - P_c(S_0^+)) + Q_{\frac{1}{2}} f_w^{up}, \end{aligned}$$

where

$$Q_{\frac{1}{2}} = -\chi(S_{\frac{1}{2}}, P_{\frac{1}{2}})T(P_1^- - P_0^+), \quad f_w^{up} = \begin{cases} f_w(S_0^+, P_0^+) & \text{for } Q_{\frac{1}{2}} \geq 0 \\ f_w(S_1^-, P_1^-) & \text{for } Q_{\frac{1}{2}} < 0 \end{cases}.$$

In calculations by elements we need to compute the following local contributions to the accumulation terms:

$$M_0 = \rho_w(S_0^+, P_0^+)S_0^+ + \rho_g(S_0^+, P_0^+)(1 - S_0^+) \quad N_0 = \rho_w(S_0^+, P_0^+)S_0^+,$$

$$M_1 = \rho_w(S_1^-, P_1^-)S_1^- + \rho_g(S_1^-, P_1^-)(1 - S_1^-) \quad N_1 = \rho_w(S_1^-, P_1^-)S_1^-.$$

To form the Jacobian, we need to compute the derivatives

$$\frac{dS_0^+}{dS_0}(S_0), \frac{dS_1^-}{dS_1}(S_1), \frac{\partial P_0^+}{\partial S_0}(S_0, P_0), \frac{\partial P_0^+}{\partial P_0}(S_0, P_0), \frac{\partial P_1^-}{\partial S_1}(S_1, P_1), \frac{\partial P_1^-}{\partial P_1}(S_1, P_1).$$

As mentioned before, here the scheme is presented for the global unknown at the interface equal to the left limiting saturation (pressure), so it is always valid:

$$S_1^- = S_1, \ \frac{\partial S_1^-}{\partial S_1} = 1, \ P_1^- = P_1, \ \frac{\partial P_1^-}{\partial S_1} = 0, \ \frac{\partial P_1^-}{\partial P_1} = 1.$$

From the transmission conditions (28) and (29) one obtains the following:

$$\frac{\partial S_0^+}{\partial S_0} = \begin{cases} 1 & \text{if } x_0 \neq x_\delta \\ \left(\frac{dP_c^{m1}(S_0)}{dS}\right) / \left(\frac{dP_c^{m2}(S_0^+)}{dS}\right) & \text{for } x_0 = x_\delta \end{cases}$$

$$\frac{\partial P_0^+}{\partial S_0} = \begin{cases} 0 & \text{if } x_0 \neq x_\delta \\ (\frac{\partial P_g^{m1}(S_0, P_0)}{\partial S} - \frac{\partial P_g^{m2}(S_0^+, P_0^+)}{\partial S}\frac{\partial S_0^+}{\partial S_0})/\omega^{m2}(S_0^+, P_0^+) & \text{for } x_0 = x_\delta \end{cases}$$

$$\frac{\partial P_0^+}{\partial P_0} = \begin{cases} 1 & \text{if } x_0 \neq x_\delta \\ \omega^{m1}(S_0, P_0)/\omega^{m2}(S_0^+, P_0^+) & \text{for } x_0 = x_\delta \end{cases}.$$

Note that when the unknowns at the interface node are selected differently, the above derivatives have to be calculated accordingly.

4 Numerical Simulations

In this section, we present numerical results based on the scheme presented in this paper. A code based on the C++ programming language, has been performed on various examples. The implementation uses the libMesh library [25] and PETSc [32] as a linear solver. The obtained results are satisfactory. The computed approximate solution satisfy the discrete maximum principle. Moreover, the front is approximated accurately. Below we present numerical simulations for three benchmark tests to demonstrate the ability of the method to approximate solutions of water-gas equations efficiently and accurately in nuclear underground waste disposal situations. All simulations were performed on a heterogeneous porous medium made of two rock types where the wetting phase (water) is incompressible and the non-wetting phase (gas) is compressible and obeys the ideal gas law.

4.1 Test Case 1

In the first test case the porous domain $I =]0, 200[$ is composed of two media such that $I = I_{m1} \cup I_{m2}$ where $I_{m1} =]0, 20]$ and $I_{m2} =]20, 200[$, so that the point $x = 20$ is an interface between the media. In this test, the source terms are equal to zero, which means that $\mathcal{F}_\alpha = 0,\ \alpha = w, g$. The duration of the simulation is $T = 10^6$ years.

The boundary conditions are set to be Dirichlet at the right part of the domain:

$$P_{w,out} = 1.0 \text{ MPa} \qquad P_{g,out} = 1.5 \text{ MPa}.$$

Phase fluxes are set on the left boundary:

$$Q_w = 0 \quad \text{and} \quad Q_g = 5.57 \cdot 10^{-6} \text{ kg/m}^2\text{/year}.$$

The initial conditions are equal to the Dirichlet conditions on the right part of the boundary. In this test case we use the van Genuchten capillary pressure ($m = 1 - \frac{1}{n}$)

$$P_c(S_e) = P_e(S_e^{-\frac{1}{m}} - 1)^{\frac{1}{n}} \quad S_e \in]0, 1] \tag{30}$$

and the van Genuchten-Mualem relative permeabilities

$$kr_w(S_e) = S_e^{\frac{1}{2}} \left(1 - (1 - S_e^{\frac{1}{m}})^m\right)^2 \tag{31}$$

$$kr_g(S_e) = (1 - S_e)^{\frac{1}{2}} (1 - S_e^{\frac{1}{m}})^{2m}. \tag{32}$$

where S_e is the effective water saturation. It is assumed that $K = cte$ in each subset of the domain. The same is valid for the porosity. The parameters for the relative permeabilities and the capillary pressures are different on each sub-domain. The temperature is taken to be fixed, $T = 303$ K. The parameters for each sub-domain are presented in Table 1. The following fluid properties are considered: $\mu_w = 1$ cP, $\mu_g = 0.009$ cP, $\rho_w = 1000$ kg/m^3. The gas density is modeled by the ideal gas law $\rho_g(P_g) = c_g P_g$, where $c_g = 0.794$ kg/m^{3}MPa.

	n -	P_e MPa	S_{wr} -	S_{gr} -	Φ -	K m^2
I_{m1}	1.54	2	0.01	0.0	0.3	10^{-18}
I_{m2}	1.49	15	0.4	0.0	0.15	$5 \cdot 10^{-20}$

Table 1: Test 1. Function parameters and rock properties.

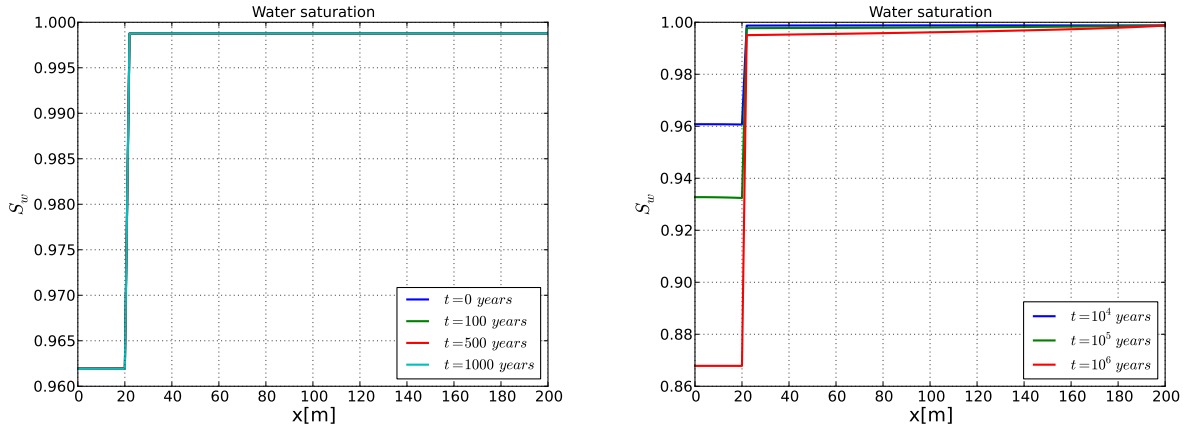

Figure 4: Test 1. Water saturation at different times.

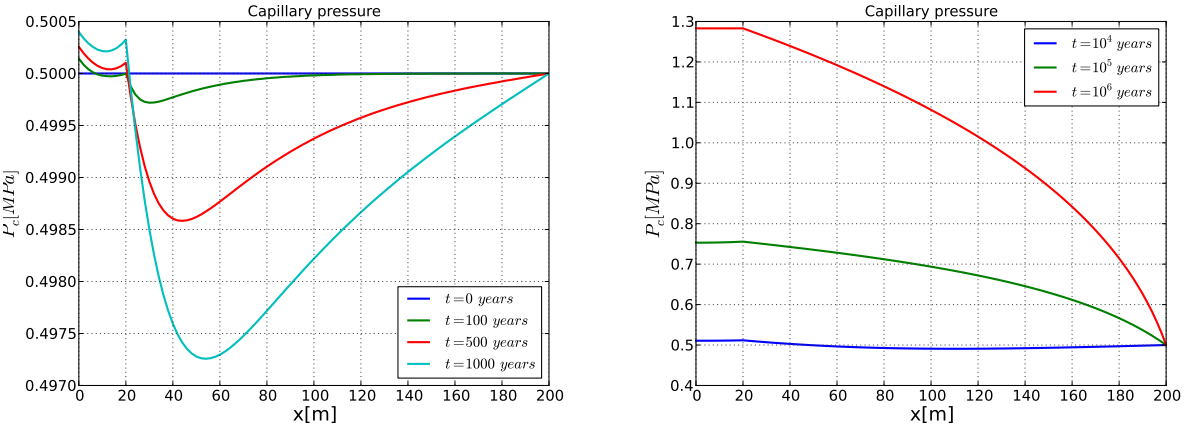

Figure 5: Test 1. Capillary pressure at different times.

In this simulation, an equidistant grid of the space domain with $\Delta x = 200$ cm is used and a time step varying from $\Delta t = 10$ years at the beginning to $\Delta t = 250$ years at the end of the simulation. The obtained results are presented in Figures 4-9. We can observe that during the first 1000 years, due to the small amount of gas (hydrogen) injected, the changes in the saturation are very small. Also, the changes in the water pressure presented in Figure 8 are not significant at the first 1000 years. The water pressure is increasing at the beginning and as one may observe in Figure 8, around the time of $5 \cdot 10^4$ years it starts

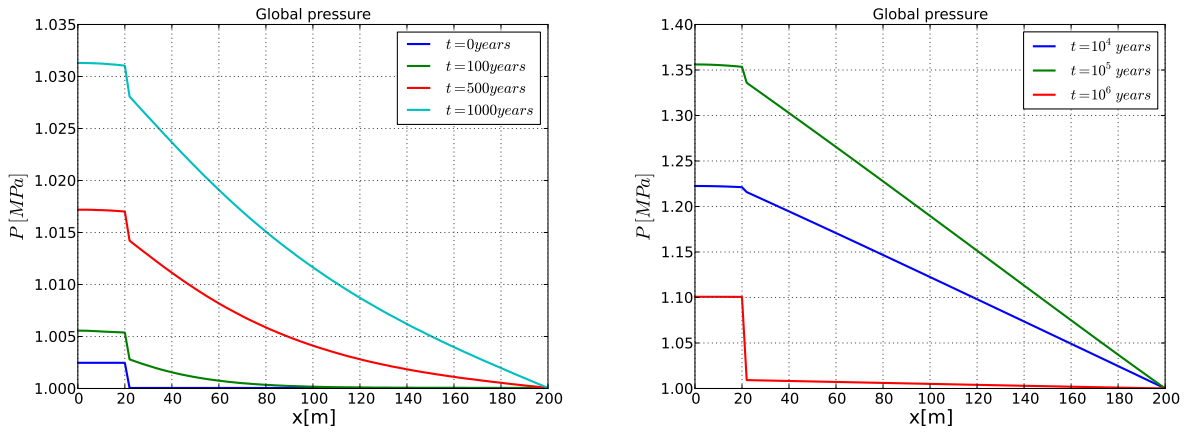

Figure 6: Test 1. Global pressure at different times.

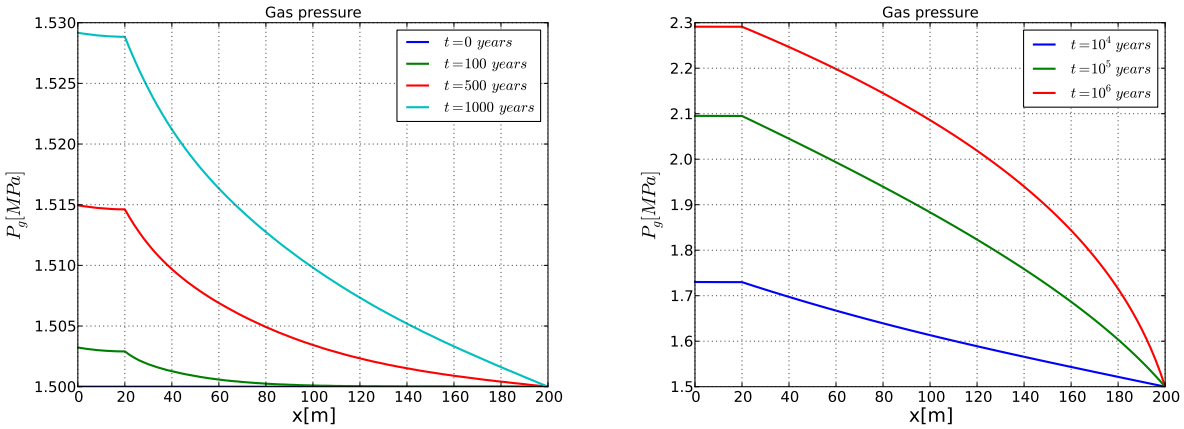

Figure 7: Test 1. Gas pressure at different times.

to decrease. At the end of the simulation, it tends to its initial value 1.0 MPa. During the whole simulation the gas pressure (presented in Figure 7) is increasing attaining the values in the range of 1.5 MPa to 2.3 MPa. The global pressure is presented in Figure 6, and its behavior is similar to that of the water pressure. The continuity condition for the gas pressure and the capillary pressure at the interface produces a discontinuity of the saturation and the global pressure at the interface.

4.2 Test Case 2

The second test case is the BOBG test case [26] - French acronyms of Engineered Barrier Geological Barrier. This test was numerically solved by other authors [2, 6]. The porous domain $I =]-0.5, 0.5[\subset \mathbb{R}$ is taken to be 1 m long. The porous domain is assumed to be composed of two media such that $I = I_{m1} \cup I_{m2}$ where $I_{m1} =]-0.5, 0]$ and $I_{m2} =]0, 0.5[$,

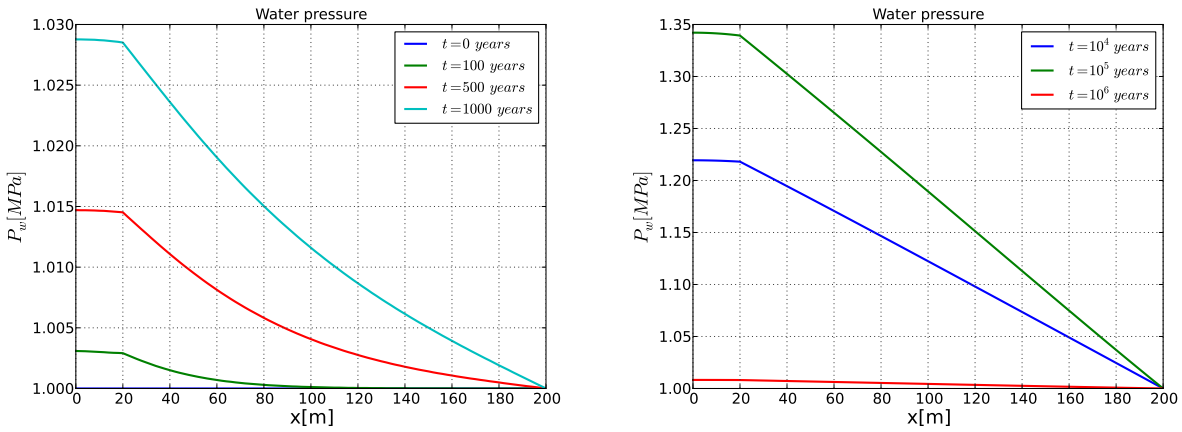

Figure 8: Test 1. Water pressure at different times.

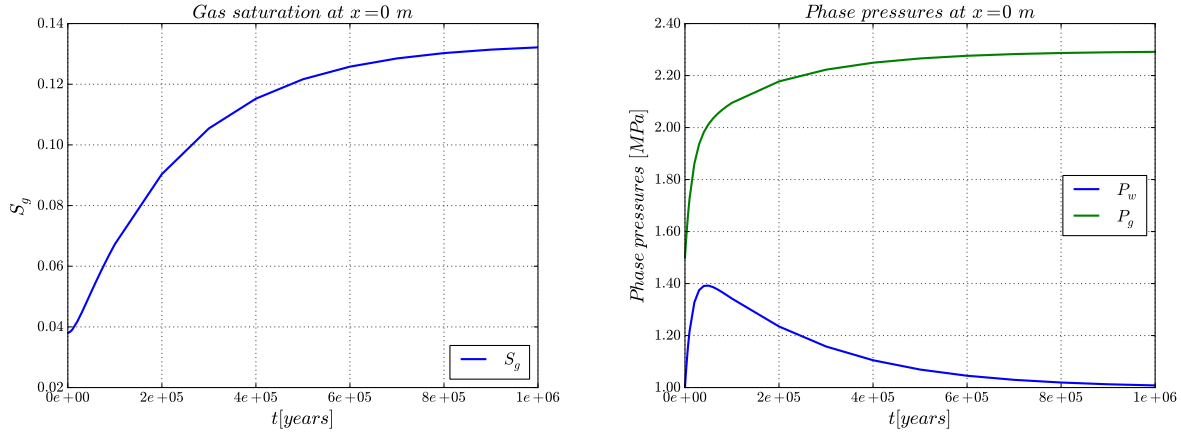

Figure 9: Test 1. Gas saturation and phase pressures on the left end of the domain.

so that the point $x = 0$ is the interface between media. In this test the source terms are equal to zero.

Phase fluxes are set to be zero at the boundary, both on the left and the right end for each phase, which means that a total flux is also set to be zero:

$$Q = Q_w = Q_g = 0 \text{ kg/m}^2/\text{s}.$$

Initially, the capillary pressure is discontinuous, and the following initial condition for the water saturation is given

$$S_w(x,0) = \begin{cases} 0.77 & \text{for } x \leq 0 \\ 1 & \text{for } x > 0 \end{cases}, \quad x \in I.$$

Regarding to the initial conditions for the gas pressure two cases are considered:
Test case 2.1

$$P_g(x,0) = 0.1 \text{ MPa}, \ x \in I.$$

From these initial conditions we obtain the initial condition for the global pressure $P = -88.8449$ MPa in I_{m1}, and $P = 0.1$ MPa in I_{m2}.

Test case 2.2

$$P_g(x,0) = \begin{cases} 0.1 \text{ MPa} & \text{for } x \le 0 \\ 0.0 \text{ MPa} & \text{for } x > 0 \end{cases}, \quad x \in \ I.$$

From these initial conditions we obtain the initial condition for the global pressure $P = -88.8449$ MPa in I_{m1}, and $P = 0.0$ MPa in I_{m2}.

In this test case the van Genuchten capillary pressure is used and the relative permeabilities are given by the following formulae:

$$S_w(P_c) = \left(1 + \left(\frac{P_C}{Pr}\right)^{\frac{1}{1-m}}\right)^{-m}$$

$$kr_g(S) = (1-S)^2(1-S^{\frac{5}{3}}), \quad kr_w(S) = (1 + A(S^{-B} - 1)^C)^{-D}.$$

It is assumed that $K = cte$ in each subset of the domain. The same is valid for the porosity. The parameters for the relative permeabilities and the capillary pressures, different on each sub-domain, are presented in Table 2. Isothermal assumption at $T = 300$ K is considered.

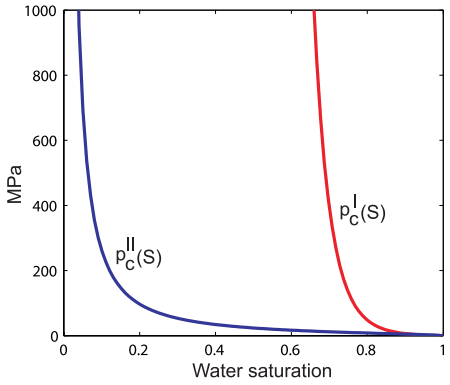

Figure 10: Test 2. Capillary pressures in the two media.

The following fluid properties are taken: $\rho_w = 1000$ kg/m^3, $\mu_w = 1$ cP, $\mu_g = 0.018$ cP, $M_g = 0.02896$ kg mol^{-1}. The density of gas is modeled by the ideal gas law $\rho_g = c_g P_g$. In numerical results presented here, in the Test case 2.1, the density of gas is scaled so that $c_g = 1.0$ kg/m^{3}MPa. In the spatial domain, an equidistant mesh is taken with the step size $\Delta x = 0.01$ m. The time steps used during the simulation are from 10^{-5} s at the beginning to the $2 \cdot 10^6$ s at the end of the simulation. The obtained results are presented

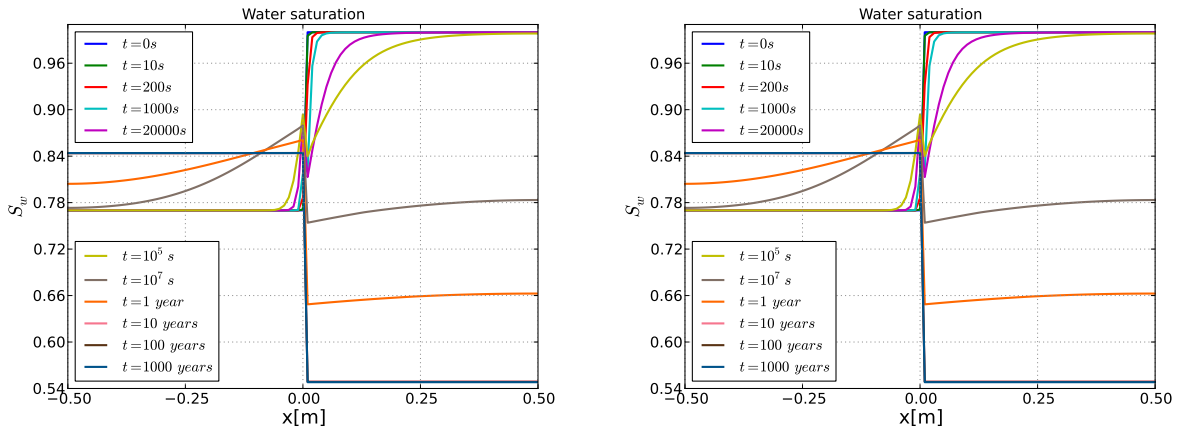

Figure 11: Test 2. Water saturation at different times for Test case 2.1 (left) and Test case 2.2 (right)

	Pr MPa	m -	A -	B -	C -	D -	Φ -	K m^2
I_{m1}	1.5	0.06	0.25	16.67	1.88	0.5	0.3	10^{-20}
I_{m2}	10	0.412	1.0	2.429	1.176	1.0	0.05	10^{-19}

Table 2: Test 2. Function parameters and rock properties.

in Figures 11-15. As shown in Figures the results for Test case 2.1 and 2.2 differ visibly only in the values of the gas pressures obtained at 10^5 s. This is also confirmed in [6].

In both cases the right part of the domain I_{m2} is initially fully saturated with water. At first, the changes of saturation are very small, the water starts to flow from the sub-domain I_{m2} to the sub-domain I_{m1}. After a certain time a change in the saturation in the region I_{m2} becomes more visible. In the region I_{m1}, the gas pressure increases near the interface, since the gas is expected to enter the domain saturated by water. As explained in [6] the volume which was occupied by water in the sub-domain I_{m2} cannot be immediately filled by gas, so in Test case 2.1, in the sub-domain I_{m2} an exact vacuum is observed. At the time of 10^5 s in both cases, the gas pressure becomes 0 MPa in the sub-domain I_{m2}, see Figure 13. After the time of 10^5 s in both test cases in the region I_{m1} the gas pressure starts to decrease from its maximum value in the vicinity of the interface. In the region I_{m2}, it starts to obtain strictly positive values, as x and t augments. In later times, it is increasing function of time in the region I_{m2}. At the end of the simulation the gas pressure tends to the value of 0.1 MPa which is the initial value that was set in Test case 2.1.

In both cases, at later times the water pressure attains constant value of around -20.0 MPa in the whole domain, because the water is mobile in the whole domain, see Figure 14.

At the beginning of the simulation variation in the saturation is higher in the sub-domain I_{m2}, than in I_{m1} because of the porosity value set. In both cases, the wetting phase

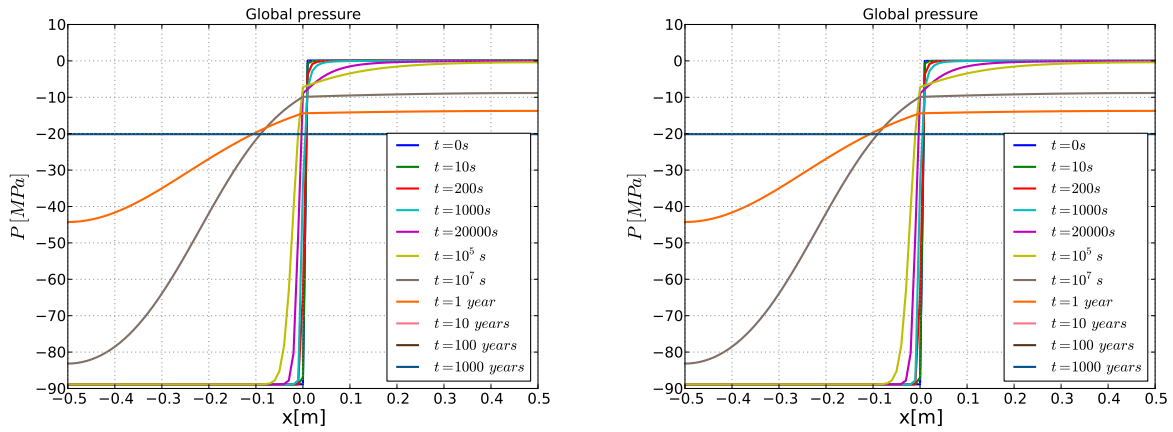

Figure 12: Test 2. Global pressure at different times for Test case 2.1 (left) and Test case 2.2 (right).

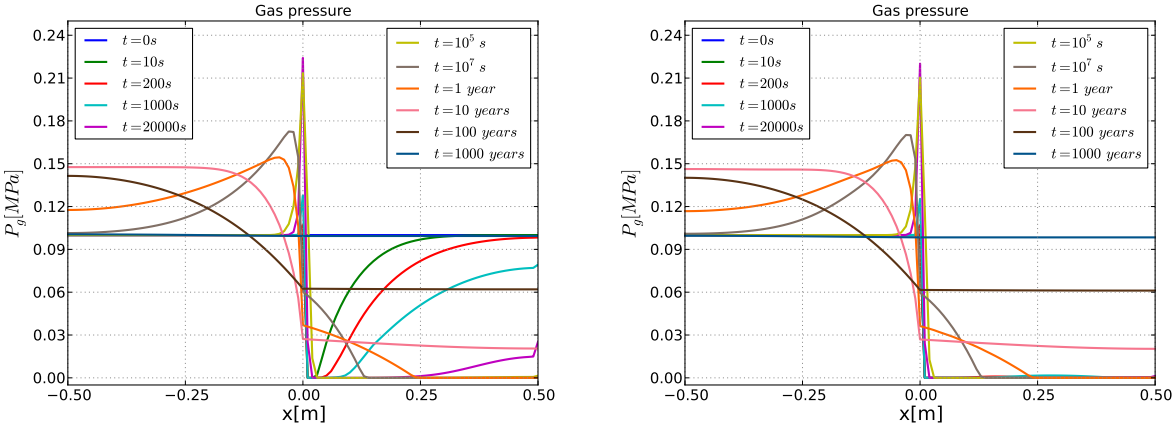

Figure 13: Test 2. Gas pressure at different times for Test case 2.1 (left) and Test case 2.2 (right).

saturation attains the value $S_w = 0.844$ on the left part of the domain, and $S_w = 0.548$ on the right part of the domain by the end of the simulation. In both cases after the time of 10^8 s, the changes in saturation are not significant.

The difference between the global pressure and the water pressure is small compared to its difference from the gas pressure. This observation is valid during the whole simulation.

4.3 Test Case 3

The third test case is considered in order to simulate the effect of the entry pressure. The porous domain $I =]0, 200[\subset \mathbb{R}$ is taken to be 200 m long. The domain is composed of two media such that $I = I_{m1} \cup I_{m2}$ where $I_{m1} =]0, 100]$ and $I_{m2} =]100, 200[$, so that the

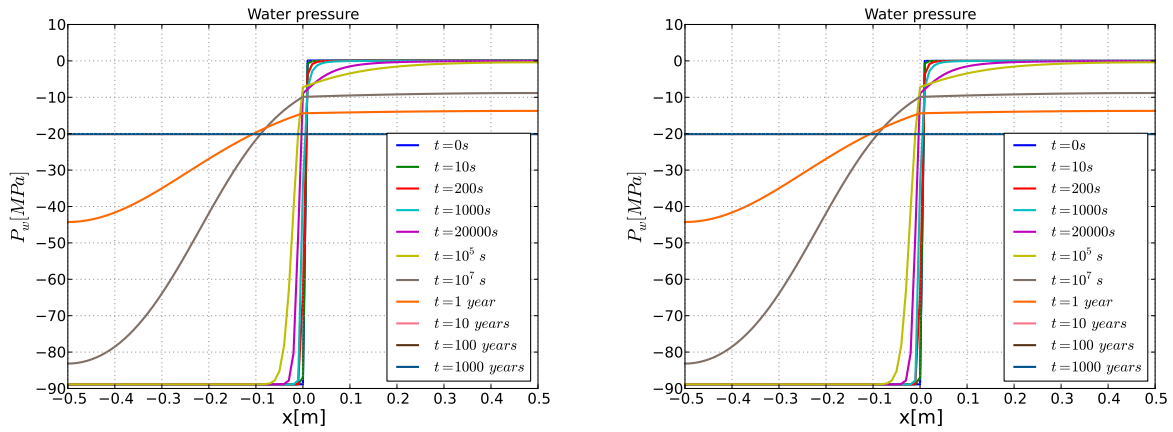

Figure 14: Test 2. Water pressure at different times for Test case 2.1 (left) and Test case 2.2 (right).

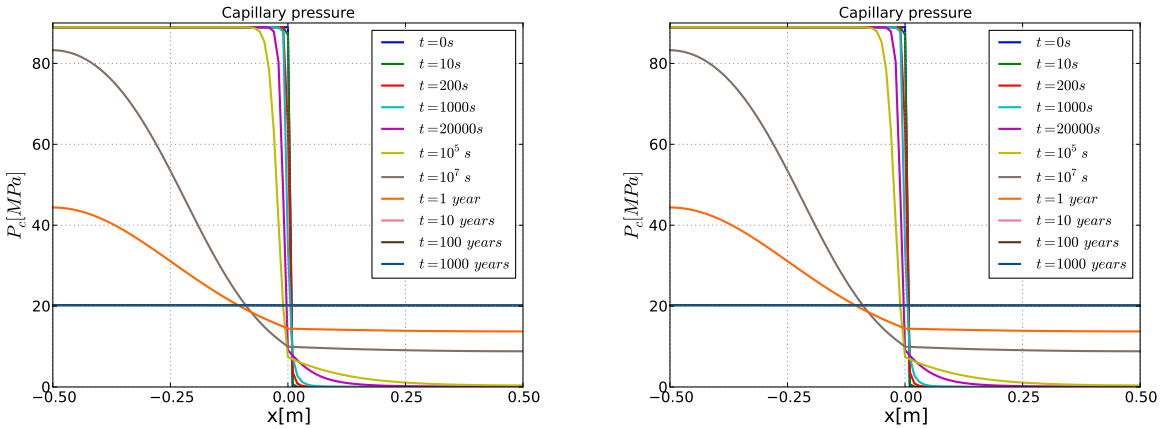

Figure 15: Test 2. Capillary pressure at different times for Test case 2.1 (left) and Test case 2.2 (right).

point $x = 100$ is the interface between the two media. In this test, the source terms are equal to zero.

The boundary conditions are set to be Dirichlet on the right boundary:

$$S_{w,out} = 1.0 \qquad P_{w,out} = 1.0 \text{ MPa}.$$

On the left boundary, phase fluxes conditions (total flux) are set:

$$Q_w = 0 \quad \text{and} \quad Q_g = 500 \text{ mg/m}^2\text{/year}.$$

The initial conditions are equal the Dirichlet conditions on the right part of the boundary. It is assumed that the porous medium is fully saturated by water and the gas is injected.

In this numerical test, we use Brooks and Corey capillary pressure

$$P_c(S_e) = P_d S_e^{-\frac{1}{\lambda}} \quad S_e \in]0,1], \tag{33}$$

and Brooks and Corey-Burdine relative permeabilities

$$kr_w(S_e) = S_e^{3+\frac{2}{\lambda}} \tag{34}$$

$$kr_g(S_e) = (1-S_e)^2 \left(1 - S_e^{\frac{2+\lambda}{\lambda}}\right) \tag{35}$$

where S_e is the effective water saturation.
It is assumed that all parameters are the same for each part of the domain: only the entry pressures differ. The temperature is assumed to be fixed, $T = 303$ K. The following

	λ -	P_d MPa	S_{wr} -	S_{gr} -	Φ -	K m^2
I_{m1}	0.5	1.9	0.0	0.0	0.3	10^{-16}
I_{m2}	0.5	2.1	0.0	0.0	0.3	10^{-16}

Table 3: Test 3. Function parameters and rock properties.

fluid properties are considered: $\mu_w = 1$ cP, $\mu_g = 0.009$ cP, $\rho_w = 1000$ kg/m^3, $c_g = 0.794$ kg/m^{3}MPa. The density of gas is modeled by the ideal gas law $\rho_g(P_g) = c_g P_g$. In this example the extended capillary pressure condition (20) is applied. This means, in this particular case, that the capillary pressure is discontinuous until the threshold saturation $S^* = 0.95119$ at the interface is reached.

In this simulation, an equidistant mesh of the space domain with $\Delta x = 200$ cm is used. For the time domain, a non-equidistant step is used, starting with $\Delta t = 10^{-2}$ s at the beginning to $\Delta t = 1$ year at the end of the simulation. Also, since only the water is mobile across the interface and consequently only the water pressure is continuous, the continuity condition is applied to the water pressure. The obtained results are presented in Figures 16-20.

In Figure 16 the water saturation is presented. As the extended capillary pressure condition is used, the saturation is equal to 1 in the sub-domain I_{m2}, until the threshold saturation is reached, which is around 7685 years. One can observe the visible changes in the saturation on the right part of the domain around 9000 years. During all the time the water and the global pressure do not differ significantly, since the water saturation is very high. The global pressure has a visible discontinuity at the interface, during the time of the simulation. As expected, the capillary pressure, and the gas pressure are discontinuous until the threshold saturation is reached at the interface. The capillary pressure is increasing, which also has the effect on increasing of the gas pressure, since the changes of the water pressure are relatively small.

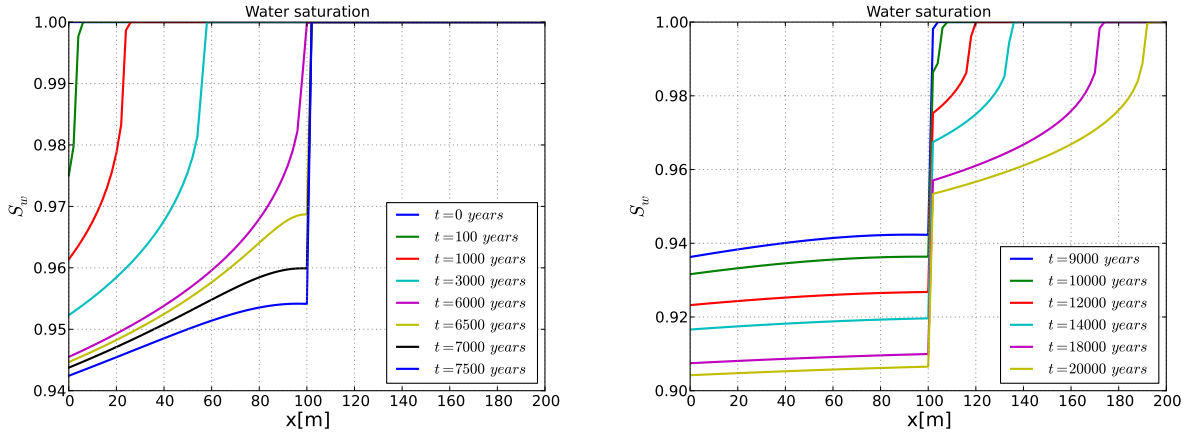

Figure 16: Test 3. Water saturation at different times.

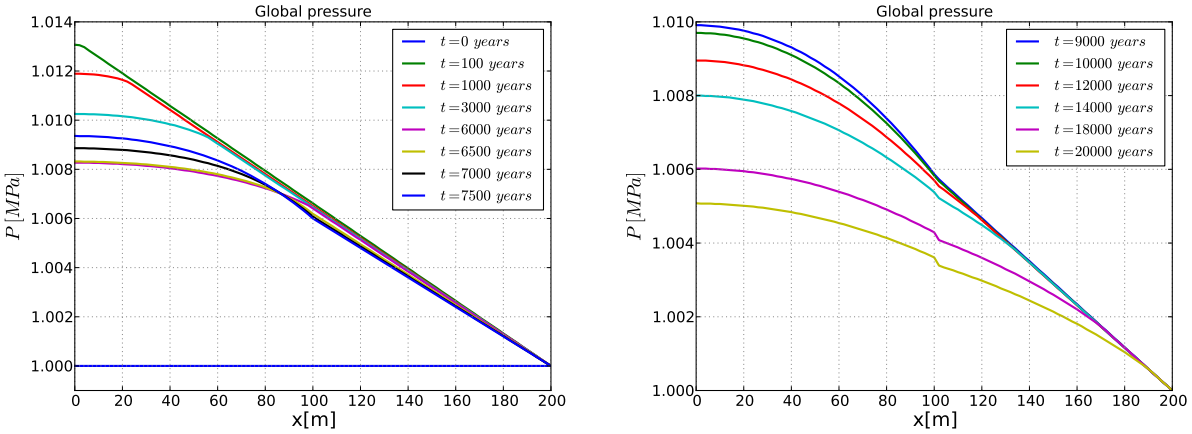

Figure 17: Test 3. Global pressure at different times.

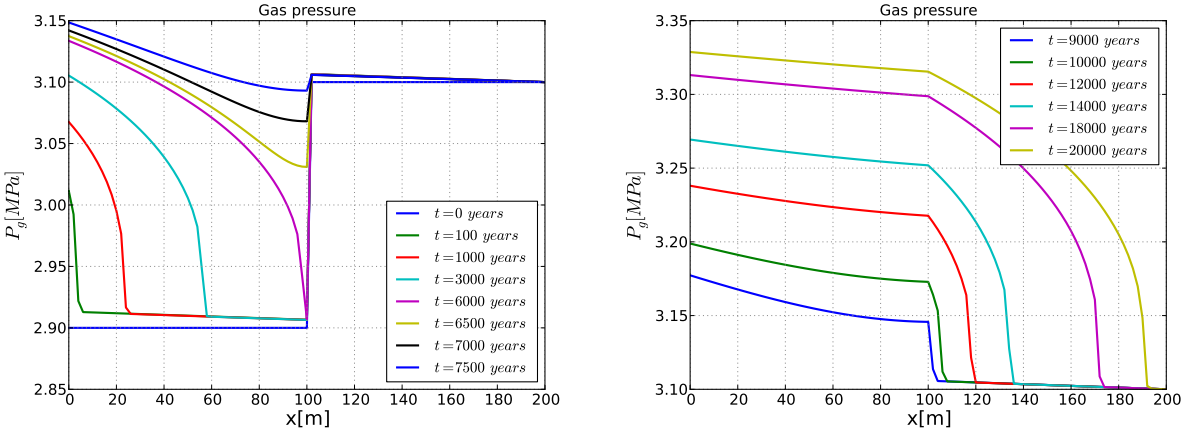

Figure 18: Test 3. Gas pressure at different times.

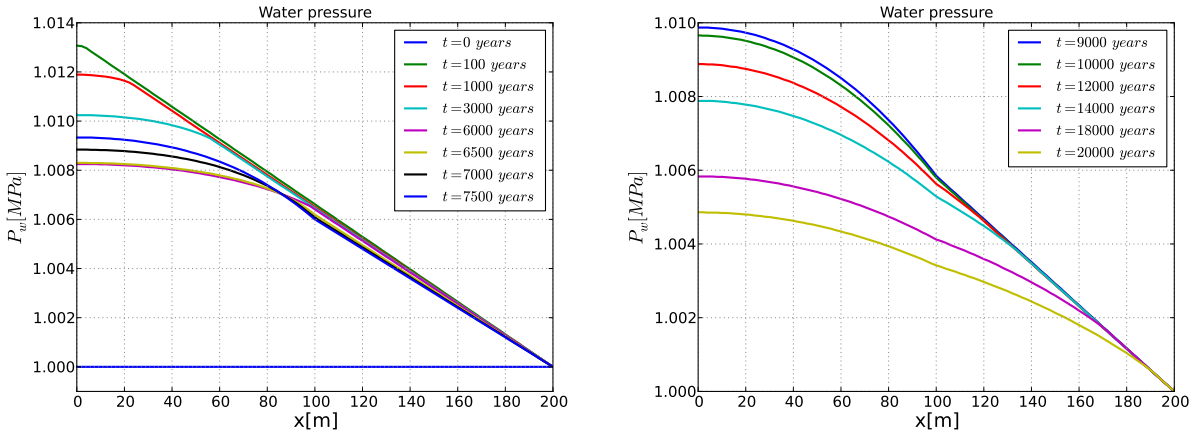

Figure 19: Test 3. Water pressure at different times.

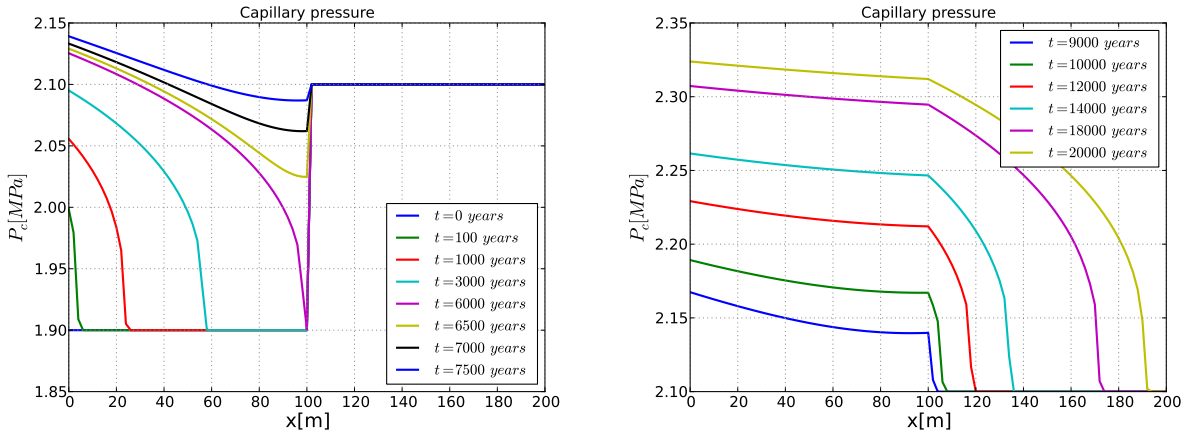

Figure 20: Test 3. Capillary pressure at different times.

5 Conclusions and Future Work

In this paper, we have presented a numerical scheme for a new immiscible, compressible two-phase flow model based on the concept of the global pressure which is fully equivalent to the original phases formulation. A special discretization at the interfaces is developed to treat media with discontinuous properties. The algorithm is then used to simulate water-gas migration related to underground waste disposal situations. The algorithm captures the complex behavior of the resulting flow. The numerical results provided in this paper follow the MOMAS benchmark guideline [26]. The results obtained for Test case 2, are close to those obtained in [2, 6], and show model applicability in the simulations with highly heterogeneous porous media. The third example shows that the model is applicable in the simulations with initially fully saturated porous media by the wetting phase, and demonstrates the significance of the entry pressure. In future work, we intend to extend the approach to more general multiphase systems with mass transfer between phases and thermal effects to the two-dimensional problem.

Acknowledgments

This research was partially supported by the AUF "Agence Universitaire de la Francophonie", Projet de Coopération Scientifique Inter-Universitaire, PHC COGITO 2011 PROJET N^0 24775XE, and the GnR MoMaS (PACEN/CNRS, ANDRA, BRGM, CEA, EDF, IRSN) France, their supports are gratefully acknowledged.

References

[1] M. Afif, B. Amaziane, On convergence of finite volume schemes for one-dimensional two-phase flow in porous media, J. Comput. Appl. Math. 145 (1) (2002), 31–48.

[2] M. Afif, B. Amaziane, Convergence of a 1-D finite volume scheme and numerical simulations for water-gas flow in porous media, Preprint submitted to Applied Numerical Mathematics (2010).

[3] B. Amaziane, M. Jurak, A new formulation of immiscible compressible two-phase flow in porous media, C. R. Mecanique 336 (7) (2008) 600–605.

[4] B. Amaziane, M. Jurak, A. Žgaljić Keko, Modeling and numerical simulations of immiscible compressible two-phase flow in porous media by the concept of global pressure, Transport in Porous Media 84 (1) (2010) 133-152.

[5] B. Amaziane, M. Jurak, A. Žgaljić Keko, An existence result for a coupled system modeling a fully equivalent global pressure formulation for immiscible compressible two-phase flow in porous media, Journal of Differential Equations 250 (3) (2011), 1685–1718.

[6] O. Angelini, C. Chavant, E. Chénier, R. Eymard, S. Granet, Finite volume approximation of a diffusion-dissolution model and application to nuclear waste storage, Mathematics and Computers in Simulation 81 (10) (2011), 2001–2017.

[7] P. Bastian, Numerical computation of multiphase flows in porous media, Habilitationsschrift, 1999.

[8] P. Bastian, R. Helmig, Efficient fully-coupled solution techniques for two-phase flow in porous media: Parallel multigrid solution and large scale computation, Advances in Water Resources 23 (3) (1999), 199–216.

[9] A. Bourgeat, M. Jurak, F. Smaï, Two-phase, partially miscible flow and transport modeling in porous media; application to gas migration in a nuclear waste repository, Comput. Geosci. 13 (1) (2009), 29–42.

[10] C. Cancès, Finite volume scheme for two-phase flows in heterogeneous porous media involving capillary pressure discontinuities, M2AN Math. Model. Numer. Anal. 43 (5) (2009), 973–1001.

[11] G. Chavent, J. Jaffré, Mathematical Models and Finite Elements for Reservoir Simulation, North–Holland, Amsterdam, 1986.

[12] G. Chavent, A fully equivalent global pressure formulation for three-phases compressible flows, Appl. Anal. 88 (10–11) (2009) 1527–1541.

[13] Z. Chen, R.E. Ewing, Fully discrete finite element analysis of multiphase flow in groundwater hydrology, SIAM J. on Numerical Analysis 34 (1997) 2228–2253.

[14] Z. Chen, G. Huan, Y. Ma, Computational Methods for Multiphase Flows in Porous Media, SIAM, Philadelphia, 2006.

[15] R. di Chiara Roupert, G. Chavent, G. Schäfer, Three-phase compressible flow in porous media: Total differential compatible interpolation of relative permeabilities, Journal of Computational Physics 229 (12) (2010), 4762–4780.

[16] C.J. van Duijn, M.J. de Neef, The effect of capillary forces on immiscible two-phase flow in heterogeneous porous media, Transport in Porous Media 21 (1) (1995), 71–93.

[17] C.J. van Duijn, M.J. de Neef, Similarity solution for capillary redistribution of two phases in a porous medium with a single discontinuity, Advances in Water Resources 21 (6) (1998), 451–461.

[18] G. Enchery, R. Eymard, A. Michel, Numerical approximation of a two-phase flow problem in a porous medium with discontinuous capillary forces, SIAM J. Numer. Anal. 43 (6) (2006) 2402–2422.

[19] A. Ern, I. Mozolevski, L. Schuh, Discontinuous Galerkin approximation of two-phase flows in heterogeneous porous media with discontinuous capillary pressures , Computer Methods in Applied Mechanics and Engineering 199 (23-24) (2010), 1491–1501.

[20] R. Fučik, J. Mikyška, M. Baneš, T. Illangasekare, Semianalytical solutions for two-phase flow in porous media with a discontinuity, Vadose Zone Journal 7 (3) (2008), 1001–1009.

[21] R. Helmig, Multiphase Flow and Transport Processes in the Subsurface, Springer, Berlin (1997).

[22] R. Helmig, R. Huber, Comparison of Galerkin-type discretization techniques for two-phase flow in heterogeneous porous media, Advances in Water Resources 21 (8) (1998), 697–711.

[23] H. Hoteit, A. Firoozabadi, Numerical modeling of two-phase flow in heterogeneous permeable media with different capillarity pressures, Advances in Water Resources 31 (2008) 56–73.

[24] R. Huber, R. Helmig, Node-centered finite volume discretizations for the numerical simulation of multiphase flow in heterogeneous porous media, Comput. Geosci. 4 (2) (2000), 141–164.

[25] B.S. Kirk, J.W. Peterson, R.H. Stogner, and G. F. Carey. libMesh: A C++ Library for Parallel Adaptive Mesh Refinement/Coarsening Simulations. Engineering with Computers, 22 (3-4) (2006), 237–254.

[26] MoMaS, Diphasique benchmarks, http://www.gdrmomas.org/ex_qualifications.html

[27] D. Nayagum, G. Schafer, R. Mosé, Modelling two-phase incompressible flow in porous media using mixed hybrid and discontinuous finite elements, Computational Geosciences 8 (1) (2004), 49–73.

[28] M.J. de Neef, J. Molenaar, Analysis of DNAPL infiltration in a medium with a low-permeable lens, Computational Geosciences 1 (1997) 191–214.

[29] J. Niessner, R. Helmig, H. Jakobs, J.E. Roberts, Interface condition and linearization schemes in the Newton iterations for two-phase flow in heterogeneous porous media, Advances in Water Resources 28 (7) (2005) 671–687.

[30] OECD/NEA, Safety of Geological Disposal of High-level and Long-lived Radioactive Waste in France, An International Peer Review of the "Dossier 2005 Argile" Concerning Disposal in the Callovo-Oxfordian Formation, OECD Publishing (2006), Available online at http://www.nea.fr/html/rwm/reports/2006/nea6178-argile.pdf.

[31] A. Papafotiou, H. Sheta, R. Helmig, Numerical modeling of two-phase hysteresis combined with an interface condition for heterogeneous porous media, Computational Geosciences 14 (2) (2010) 273–287.

[32] PETSc, http://www.mcs.anl.gov/petsc/petsc-as/.